JOURNAL OF PROPULSION AND POWER
Vol. 23, No. 5, September–October 2007

Experimental Characterization of a Micro-Hall Thruster

Tsuyohito Ito,* Nicolas Gascon,† W. Scott Crawford,‡ and Mark A. Cappelli§
Stanford University, Stanford, California 94305-3032

DOI: 10.2514/1.27140

The operation and performance of a micro-Hall thruster are characterized. The thruster is coaxial in design, with a 0.5 mm channel width and 4 mm outer diameter. The magnetic circuit includes a samarium cobalt permanent magnet generating approximately 0.7 T at the exit plane and 1 T inside the channel. Operation with a commercial hollow cathode neutralizer is achieved in the 10–40 W power range with an anode flow rate of 0.12–0.20 mg/s of xenon. The measured thrust is in the range of 0.6–1.6 mN for an anode flow rate of 0.17–0.20 mg/s and an applied voltage of 110–275 V. Anode thrust efficiency and specific impulse are in the range of 10–15% and 300–850 s, respectively, for the same conditions. Relatively broad ion energy distributions and large beam divergence are observed from an analysis of the plume using a retarding potential analyzer and ion current probe. The discharge exhibits the characteristic Hall thruster "breathing mode" instability in the 35–70 kHz frequency range.

Nomenclature

E_i	=	ion energy
e	=	elementary electric charge
F	=	thrust
f	=	breathing mode frequency
g_0	=	universal gravitation constant
I_d	=	discharge current
I_{sp}	=	anode specific impulse
J_i	=	total ion current measured in the plume
$j_{i\theta}$	=	angle-dependent ion current
L	=	characteristic size of discharge
m_i	=	ion mass
$\dot{m}$	=	anode mass flow rate
T_e	=	electron temperature
U_d	=	discharge voltage
v_i	=	ion velocity
v_n	=	neutral velocity
η	=	anode thrust efficiency
ϕ_c	=	cold probe floating potential
ϕ_e	=	emissive probe floating potential
ϕ_p	=	plasma potential

I. Introduction

HALL discharge plasma accelerators, also called Hall thrusters, have been studied for satellite propulsion since the early 1960s [1,2]. In a typical Hall thruster [3], a magnetic field is applied across an electrical discharge sustained within a cylindrical dielectric channel, which allows for closing the electron drift current in the Hall ($E \times B$) direction. The anode is located at the base of the channel, and serves also as the source of propellant. A cathode external to the channel provides electrons that migrate toward the anode across the predominantly radial magnetic field, which typically peaks at 10–20 mT near the channel exit. For such a magnetic field strength, and at the relatively low channel pressure (~0.1 Pa), the electrons are highly magnetized, and have a Larmor radius of about 1 mm. Although the precise mechanism for electron demagnetization is unknown, it is now widely accepted that the cross-field electron current is somewhat anomalous, varying in strength depending on the location within the channel [4,5]. The partial confinement of the electrons in the strong magnetic field region gives rise to enhanced ionization due to the increased effective residence time of the electrons. This confinement also serves to concentrate the region of potential drop. The ions created in the confinement region are negligibly affected by the magnetic field because of their large mass, and are rapidly accelerated out of the channel by the self-consistent electric field. The ion space charge is neutralized in the plume by additional electrons emitted by the cathode. Modern Hall thrusters operate in the 0.2–100 kW power range, with thrust efficiencies (propulsive power over input power) in the 30–70% range, and specific impulses (thrust over propellant flow rate) in the 1000–4000 s range.

The past decade has seen an increased interest in scaling Hall thrusters down to the 10–100 W range for use on power-limited and small satellites [6]. A prototype Hall thruster with a 20 mm channel outer diameter was operated by Guerrini et al. in the 30–130 W range [7]. The measured thrust was 1–4 mN, and the efficiency was 7–9%. The same power range was explored with a smaller device (4.8 mm channel outer diameter) by Khayms and Martinez-Sanchez, who also presented a detailed analysis of scaling laws for Hall thrusters [8,9]. An important result of their study is that the characteristic dimension of the discharge L should scale as the discharge power $I_d \cdot U_d$, and the magnetic field applied to the plasma should scale as $1/L$. In turn, the discharge power density (power per unit area) is also expected to scale as $1/L$. If the conventional annular channel geometry is kept, a reduction in scale thus leads to significant constraints on the central part of the thruster (inner channel wall and pole piece) due to the limited space and increased thermal stress. Indeed, the thruster described in [9] could not be operated for an extended time at optimal conditions because of discharge chamber overheating, and the measured efficiency was relatively low (4–6% for a thrust of 0.4–1.8 mN).

Various concepts were proposed to address these issues. Schmidt et al. reported encouraging results with a linear channel Hall thruster [10], although this type of discharge is inherently less efficient than the annular one because of the electron Hall current striking the sidewall instead of flowing in a closed annular drift. Another option is to recess the central part of the annular channel, as in the so-called cylindrical Hall thruster studied by Smirnov et al. [11–13]. One such thruster, which had a 26 mm outer diameter channel, was successfully operated in the range of 50–300 W with an efficiency of 15–32% and thrust of 2.5–12 mN.

In this paper, we evaluate the operation and performance of a micro-Hall thruster, which has been originally developed for use as a low-power (10–40 W), magnetized microdischarge (4 mm outer

Received 8 August 2006; accepted for publication 9 June 2007.

*Postdoctoral Scholar, Mechanical Engineering Department, Building 520; currently Graduate School of Engineering, Osaka University, 2-1 Yamadaoka, Suita, Osaka 565-0871, Japan. Member AIAA.

†Research Associate, Mechanical Engineering Department, Building 520. Member AIAA.

‡Research Assistant, Mechanical Engineering Department, Building 520.

§Professor, Mechanical Engineering Department, Building 520. Member AIAA.

diameter channel) ion source [14]. The channel geometry is annular, but as described in Sec. II, we use a dielectric diamond ceramic to cover and protect the central magnet pole piece and water-cooling at the iron base for better thermal management. In Sec. III, we present the general operation of this micro-Hall thruster, investigate the thruster plume with an ion probe (ion current density), a retarding potential analyzer (ion energy distribution function), an emissive probe (plasma potential), and we directly measure thrust to estimate the specific impulse and efficiency.

II. Experiments

A. Test Facility

Two vacuum facilities were used for our experiments. The plume characterization was carried out in a test facility consisting of a nonmagnetic stainless steel chamber approximately 0.6 m in diameter and 1.2 m in length. High vacuum conditions in the chamber were obtained with a single-stage 50-cm-diam cryogenic pumping system (CVI, model TM500). The base pressure of the facility was $1 \cdot 10^{-4}$ Pa, as measured by an ionization gauge uncorrected for xenon. Thruster testing at xenon flow rates of 0.12–0.20 mg/s resulted in chamber background pressure of $1 \cdot 10^{-3}$ Pa. Thrust measurements were carried out in a larger test facility consisting of a nonmagnetic stainless steel chamber approximately 1.5 m in diameter and 3.3 m in length, and a two-stage cryopump (CVI, model TM1200). The pressure during the thrust measurements was approximately $5 \cdot 10^{-4}$ Pa. Research grade (99.995%) xenon was used for the main thruster discharge and for the hollow cathode, with mass flow controller accuracy within 1% of the total flow rate [1.25–2 sccm (standard cubic centimeters per minute), or 0.12–0.2 mg/s Xe at the anode].

B. Micro-Hall Thruster

A schematic illustration of the micro-Hall thruster is shown in Fig. 1, and a photograph of the actual thruster is shown in Fig. 2. The magnetic circuit incorporates a ring-shaped samarium cobalt (SmCo) permanent magnet in conjunction with a high-purity iron circuit. The outer diameter of the magnet is 14 mm, the inner diameter is 4 mm, and the thickness is 3 mm. The outer diameter of the iron core, which is also the inner diameter of the channel, is 3 mm, and the channel width is thus $w = 0.5$ mm. The metal part of the channel (magnet and iron) is at anode potential, and its depth is 3 mm. The magnet ring is covered with 230 μm of alumina ceramic, and the central pole piece is covered with a 3-mm-diam, 400 μm-thick, polycrystalline diamond disk. Note that both the alumina ring and the diamond disk are dielectric, and in this way, the last half-millimeter of the channel combined with the large upstream chamber at anode potential resembles that of a classical stationary plasma thruster design. The

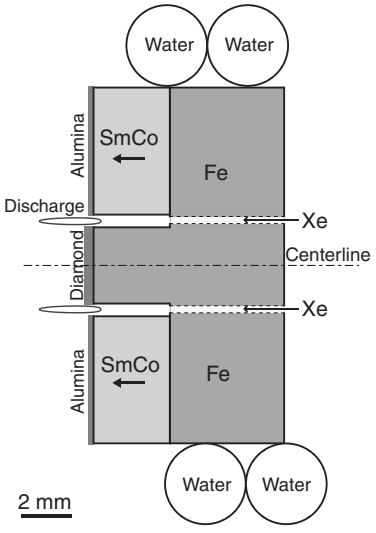

Fig. 1 Schematic of the micro-Hall thruster.

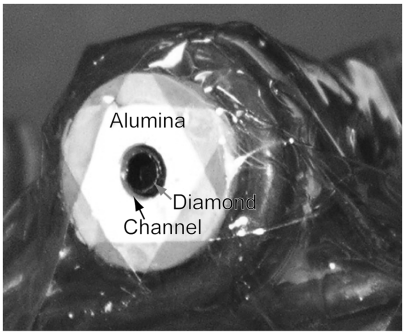

Fig. 2 Photograph of the micro-Hall thruster.

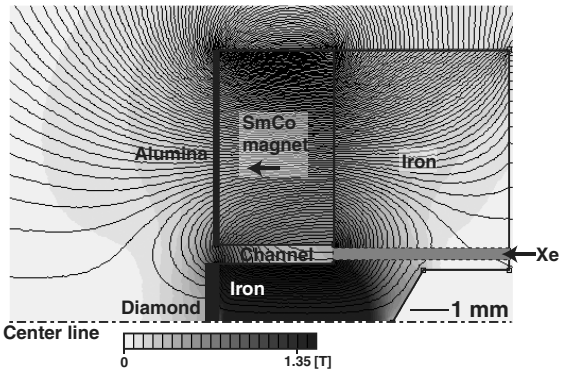

Fig. 3 Simulations of the micro-Hall thruster vacuum magnetic field.

magnetic field generated by the thruster is predominantly radial near the exit of the channel, as verified by simulations for this circuit carried out using a two-dimensional axisymmetric finite element solver [15]. The magnetic field strength near the exit of the channel (surface of the alumina insulator) is ~0.7 T and the maximum strength in the channel is approximately 1 T (see Fig. 3).

The thruster main discharge is powered by a Sorensen SCR600-1.7. Anode current oscillations are monitored by measuring the voltage across a 4Ω shunt resistor in series with the discharge. The ion plume electric charge is neutralized with a commercial hollow cathode (Ion Tech, Inc., HCN-252) operating with a flow of 0.16 mg/s of xenon and located 1 cm downstream and 4 cm off the axis of the channel. Note that in this paper, the cathode xenon and electrical power consumption are not taken into account in calculating the thruster performance. During thruster operation, to prevent overheating, the iron base of the channel is water-cooled.

C. Plume and Performance Characterization

The plume is characterized by measuring the ion energy distribution and the total ion current at various locations. A guarded planar ion probe, 3 mm in diameter and biased to −30 V to repel the electrons, is used to measure the ion current distribution and total ion current in the plume. The ion current measurements are performed 22 cm downstream of the channel exit. The ion energy distribution is characterized with a miniaturized retarding potential analyzer (RPA), with a 4 mm entrance aperture. The outermost grid of the RPA is electrically floating, the electron repelling grid is set to a potential of −25 V, and the ion retarding grid is swept to a potential of up to +350 V. The collector is coated with a graphite emulsion to reduce secondary electron emission. The transmitted ion current incident onto the collector is recorded with a picoammeter (Keithley 485). More details on our miniaturized RPA are presented in [16]. For the ion energy measurements, the entrance of the RPA is located 7 cm downstream of the channel exit. Plasma potential measurements are required for a complete analysis of the RPA data; they are obtained with an emissive probe at the same location. The main component of the emissive probe is a 150-μm-diam heated tungsten wire coil (five turns). The ion probe, RPA, and emissive

probe are mounted on a stepper motor-controlled rotational stage for angle-resolved measurements.

Performance is evaluated through direct- and indirect-thrust measurements. The direct-thrust measurements use an inverted pendulum-type balance, which includes an electromechanical damper for filtering the oscillations induced by the vacuum pumping system, and is water-cooled to minimize thermal drift during thruster operation. Calibration can be performed in situ at regular intervals using an electric motor, pulleys, and several weights of known masses (within 10^{-4} relative uncertainty). The thrust signal is linear within 1% tolerance and the system is capable of detecting horizontal forces down to ~0.1 mN. More details on the thrust stand can be found in [17]. Thrust is also calculated using the results of the ion current and energy distribution measurements in the plume.

III. Results and Discussion

A. Micro-Hall Thruster Operation

In all the measurements presented here, the discharge was operated in voltage-limited mode. Figure 4 shows a photograph of the micro-Hall thruster during operation. The discharge generates an intense blue emission most likely due to excited xenon ions. The light emission from the discharge appears to be fairly uniform around the coaxial channel. Discharge instabilities precluded operation below about 0.11 mg/s of anode flow. The discharge stability at higher flow rates (0.12–0.15 mg/s) was influenced by a slow thermal drift, and although the discharge was sufficiently stable for documenting current-voltage characteristics, the operating regime was found to change for longer running times (~20 min). The *I-V* curves, which are illustrated in Fig. 5, are somewhat typical of Hall thruster discharges [3]. For the higher range of xenon flow rates (0.17–0.20 mg/s), the inflection that is observed in the *I-V* curves (e.g., 0.20 mg/s, ~150 V) and the higher voltage points are associated with a high propellant utilization efficiency (>80%, see next section), i.e., the ion current is saturated. However, the characteristics do not saturate, contrary to what is commonly observed in modern Hall thrusters [18], suggesting that a supplemental electron current is present in the discharge. Several factors could contribute to explaining this higher than expected electron flow: the presence of multiply charged ions (see next section), high near-wall conductivity resulting from the alumina ring's high secondary electron emission yield [19], and plasma instabilities caused by the high magnetic field and negative field gradient near the anode [20].

For all the operating conditions investigated here, the discharge current exhibited strong oscillations that can be associated with the so-called breathing mode bulk plasma instability [21]. Figures 6 and 7, respectively, show oscillograms and spectral analysis of the discharge current. The observed oscillations are characterized by sharp fundamental modes in the 35–70 kHz range, with less intense harmonics. It should be noted that similar oscillations were also observed when the thruster was operated with a wire filament instead of a hollow cathode as neutralizer [16].

The breathing mode in Hall thrusters was analyzed with a predator–prey instability model as described by Fife [5], and the resulting scaling for the frequency

$$f \propto \frac{\sqrt{v_i v_n}}{L} \tag{1}$$

where v_i and v_n are the ion and neutral fluid velocities, respectively, and L is the characteristic length of the ionization/acceleration zone. In the case that v_n and L do not vary significantly, this leads to $f \propto v_i^{0.5} \propto U_d^{0.25}$. This trend was observed in the flight-qualified SPT-100 thruster [18], but in our case, the frequency (shown in Fig. 8) rises more steeply, with a voltage exponent of ~0.6. This discrepancy cannot be explained by a shortening of the ionization/acceleration when the discharge voltage is increased, as this is contradicted by the results that will be presented in Sec. III.C.

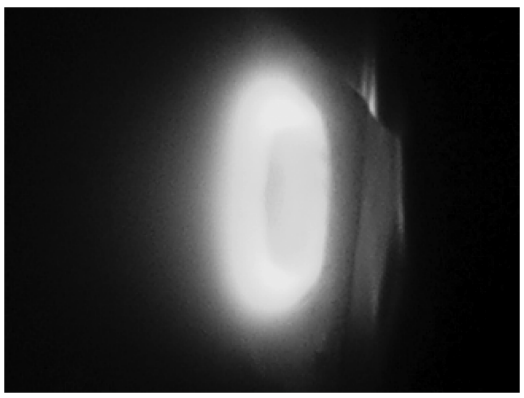

Fig. 4 Photograph of the micro-Hall thruster during operation.

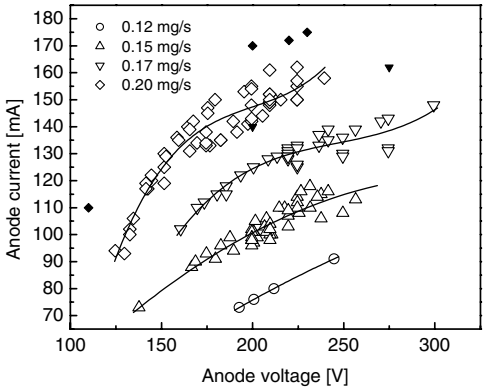

Fig. 5 Voltage-current characteristics. Note: solid symbols are for values observed during direct-thrust measurements.

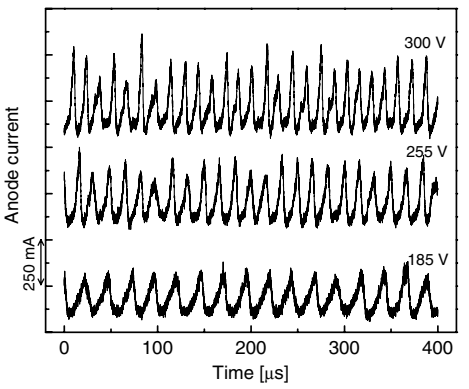

Fig. 6 Oscillograms of discharge current. Xenon flow rate is 0.17 mg/s.

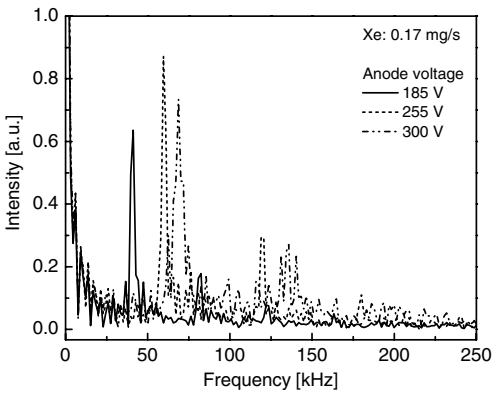

Fig. 7 Low-frequency spectral analysis of the discharge current.

B. Ion Current Measurement

The results of plume ion current measurements are shown in Fig. 9. The distributions are nearly symmetrical, perhaps slightly affected by the cathode neutralizer, which is located on the negative angle side of the scale shown. A large plume divergence, with a half-width at half-maximum (HWHM) of ∼80 deg, was observed at all operating conditions. The peak density is located near 30–50 deg (i.e., off axis). In contrast, the 1 kW level SPT-100 thruster has a peak current density located at the center of the plume and the HWHM is about 10 deg [22]. It is interesting to note that in high-voltage/low-flow operation, the maximum of current density seems to be shifted to greater angles (see Fig. 9a), which could be related to a shift of the ionization/acceleration zone away from the channel. It is unclear, however, why the current distribution variations with discharge voltage seem to be opposite for the lower flow case (0.17 mg/s, Fig. 9a) and the higher flow case (0.20 mg/s, Fig. 9b); a result that continues to be examined experimentally.

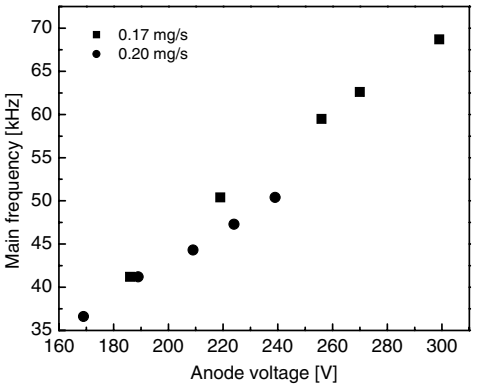

Fig. 8 Mean fundamental breathing mode frequency as a function of the discharge voltage.

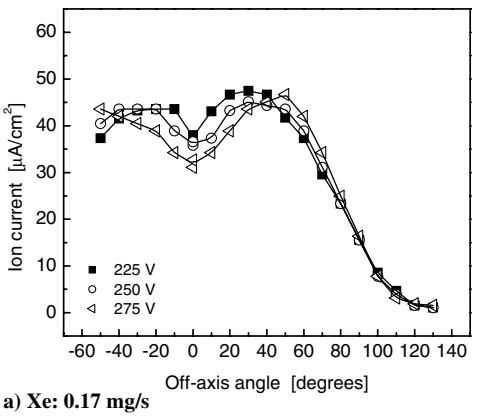

a) Xe: 0.17 mg/s

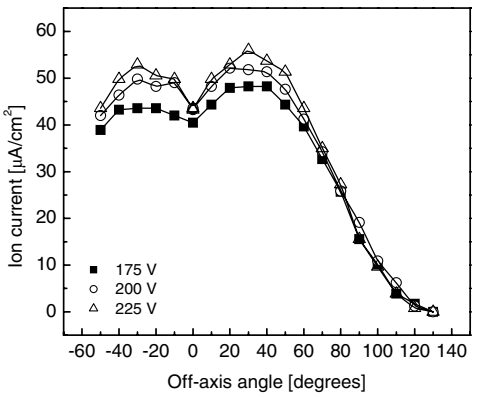

b) Xe: 0.20 mg/s

Fig. 9 Ion current distributions measured at 22 cm downstream from the anode surface.

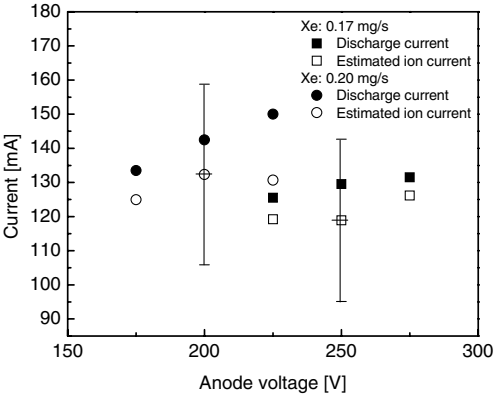

Fig. 10 Discharge and ion current as a function of the discharge voltage. Note: error bars (shown only on maximum or minimum points) are based on the estimated 20% error in ion current.

We can obtain the total ion current by spatial integration over the subtended solid angle of the distribution. The variation in the total ion current with voltage is shown in Fig. 10. The estimated uncertainty in the total ion current was at most ∼20%. Also shown in this figure are the discharge currents, for comparison. The discharge efficiencies, defined by the ratio of total ion current to discharge current (J_i/I_d), are in the range of 85–95%, as shown in Fig. 11. Also shown in this figure are the utilization efficiencies, defined by the ratio of ion mass flow to injected neutral mass flow, and calculated using the ion current measurements assuming that all the ions are singly charged. Utilization efficiencies higher than one (e.g., at 275 V discharge voltage, 0.20 mg/s propellant flow rate) reveal the presence of multiply charged ions in the plume. This could contribute to the observed increase in efficiency with discharge voltage, as the proportion of multiply charged ions should also increase.

C. Ion Energy Measurement

In the ion energy measurements, the retarding grid potential of the RPA was set relative to ground (vacuum chamber) potential. A proper analysis of the ion energy distribution requires a correction for the local plasma potential, which was measured with an emissive probe. At the RPA location (7 cm away from the channel exit plane), the floating potential of the probe was found to be independent of the thruster operating conditions, both in the cold and emissive (hot) regimes. The measured cold probe potential ϕ_c was about −20 V and the emissive probe potential ϕ_e was about 10 V, with slightly higher values near the centerline than at high angles (2 V maximum difference). It is possible to estimate the local electron temperature and the plasma potential [12,23–25]. Assuming, as in [12], that the electron energy distribution function is Maxwellian, the resulting temperature and plasma potential are

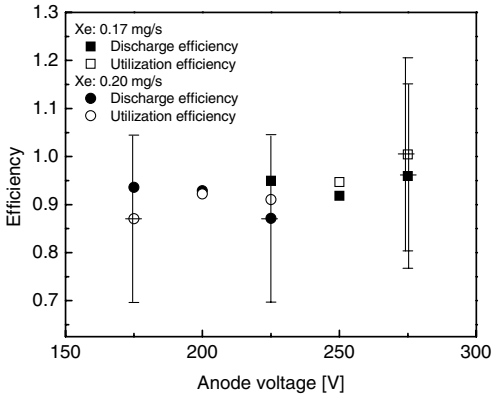

Fig. 11 Discharge and utilization efficiencies as a function of the discharge voltage. The effect of multiply charged ions is neglected. Note: error bars are based on the estimated 20% error in ion current.

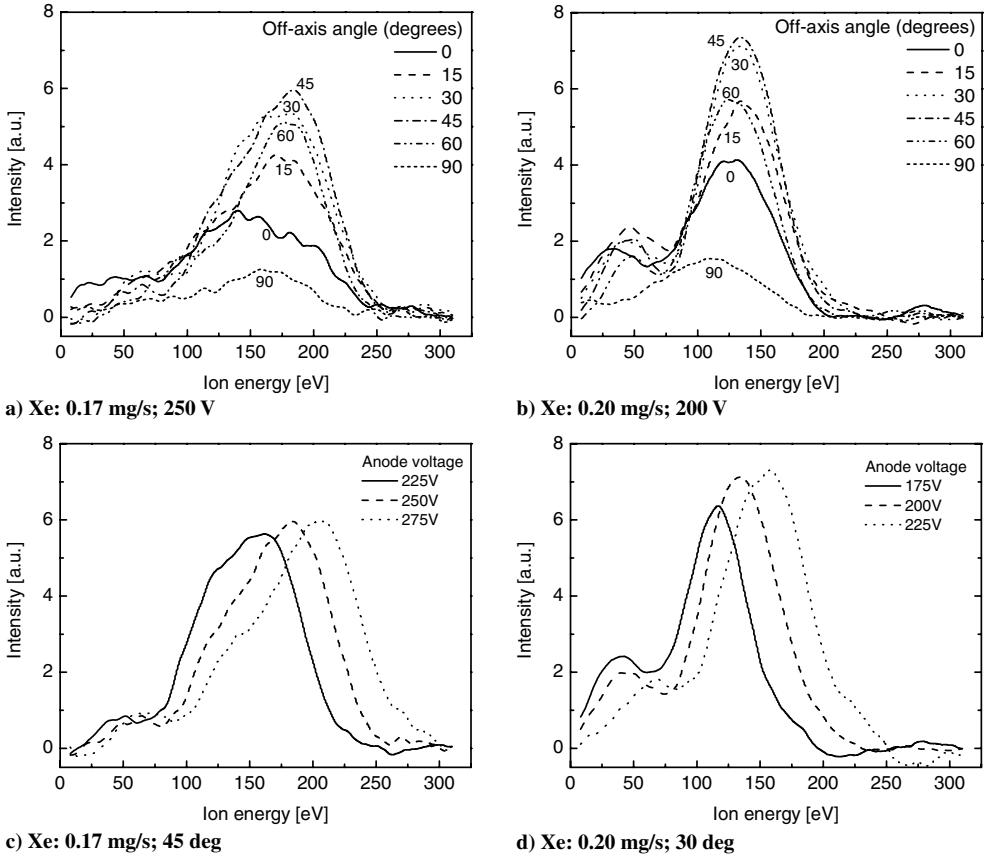

Fig. 12 Examples of ion energy distributions: a–b) angle dependence on xenon flow rate; c–d) anode voltage dependence on Xe flow rate. Note: energy is shifted from the observed value based on the ground potential by a plasma potential of 20 V.

$$T_e = \frac{\phi_e - \phi_c}{4.27} \approx 7 \text{ eV} \qquad \phi_p = \phi_e + 1.5T_e \approx 20 \text{ V}$$

Examples of ion energy distributions (corrected for an estimated plasma potential of 20 V) are shown in Fig. 12. For every distribution, the main peak is located about 60 V lower than the discharge voltage. This is in part a consequence of the energy invested in ionizing the propellant (a minimum of 12.1 eV is needed for producing XeII from the ground state of XeI), and of a significant proportion of ions that are created at a lower electric potential than the anode. It is interesting to note that the 60 eV energy deficit seems to be independent of the operating conditions, which may indicate that the shape and position of the ionization/acceleration zone do not change significantly.

Most ion energy scans (more noticeably at higher mass flow rate) exhibit a secondary peak in the range of 30–70 eV. This low-energy peak was also observed in simulations of the Hall thruster using a two-dimensional hybrid (particle-in-cell/fluid) model and was attributed, in one case, to the dynamic shift between the ionization region and the acceleration region during the breathing mode cycle [26], and in another case to charge-exchange collisions between the ions in the beam and neutral xenon emitted by the hollow cathode [27]. In our measurements, this low-energy peak may also reflect the presence of charge-exchange collisions with nonionized xenon coming from the anode, because it appears to be weaker for operation at lower anode flow rates.

The shape of the main peak is relatively broad in comparison to what is seen in larger, higher power thrusters [28–30], as shown in Fig. 13. This and the large plume divergence seen in the ion current measurements (Sec. III.B) suggest that the ionization zone is broader relative to the acceleration zone, compared with what is seen in optimized Hall thruster designs.

D. Thrust and Efficiency

Although the thrust stand was configured with flexures that were more appropriate for larger-size thrusters (∼1 kW design), direct-thrust measurements were performed despite a relatively large uncertainty of ∼0.15 mN for comparison to indirect measurements based on the ion current and ion energy distribution. From the angle-dependent energy distribution and the angle-dependent ion current $j_{i\theta}$, we can estimate the thrust F as follows:

$$F = \int_0^{\pi} \frac{j_{i\theta} m_i}{e} \left\langle \sqrt{\frac{2E_i}{m_i}} \right\rangle_{\theta} \pi \sin(2\theta)\, \mathrm{d}\theta$$

where E_i and m_i are the ion energy and mass, respectively, and e is the elementary electric charge. It has been assumed that the

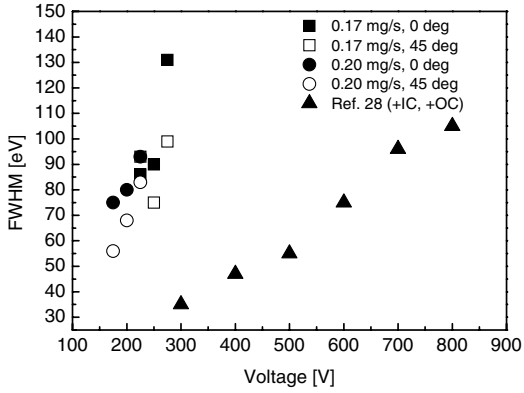

Fig. 13 Width of the ion energy distribution (primary peak) as a function of discharge voltage. Also shown are the widths measured in a 5 kW thruster [28].

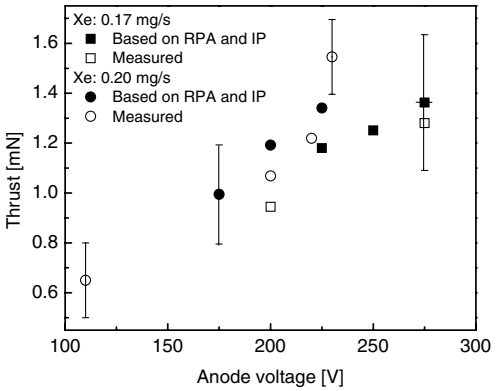

Fig. 14 Thrust as a function of the discharge voltage. Note: error bars are based on estimated 20% error in ion current and 0.15 mN uncertainty associated with direct-thrust measurements.

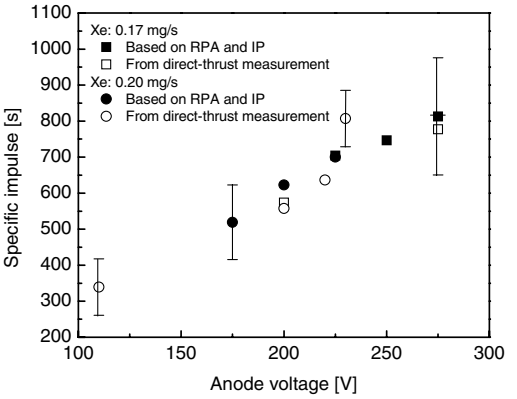

Fig. 16 Anode specific impulse as a function of the discharge voltage.

contribution to the thrust from the flow of neutrals is negligible. The results of direct- and indirect-thrust measurements are compared in Fig. 14. The thrust was found to be in the range of 0.6–1.6 mN for 0.20 mg/s anode flow rate and 110–225 V discharge voltage, and 0.9–1.3 mN for 0.17 mg/s anode flow rate and 200–275 V discharge voltage. The direct-thrust measurements are found to be in reasonable agreement with those estimated from plume parameters, but it should be noted that the discharge current monitored during the direct-thrust measurements in the larger vacuum facility are slightly higher (by ∼10%) than the discharge current observed during ion current and ion energy measurements in the smaller (and higher backpressure) vacuum facility, as shown in Fig. 5. This was unexpected, because at higher facility pressure, the background gas artificially increases the propellant flow in the channel, which tends to result in a higher thrust. The exact cause for this surprising result has not yet been identified, although it could be due to a combination of the various uncertainties of measurement (thrust stand accuracy, asymmetry of the plume) and of the impact of the maintenance performed on the thruster between the two tests (seal replacement).

From the direct- and indirect-thrust measurements, the anode thrust efficiency η and the anode specific impulse I_{sp} can be calculated:

$$\eta = \frac{F^2}{2\dot{m} \cdot U_d \cdot I_d}; \qquad I_{sp} = \frac{F}{g_0 \dot{m}}$$

The variation in thrust efficiency with discharge voltage is shown in Fig. 15. Thrust efficiency is seen to increase with increasing voltage, as expected, and is found to be in the range of approximately 10–15% for the voltage range examined here. This efficiency is higher than those reported for the 50 W power Hall thruster [8,9], and one contributing factor might be that our thruster is water-cooled. Yet the efficiency remains much lower than in 1 kW class Hall thrusters like the SPT-100 (in which it is about 50%) [18].

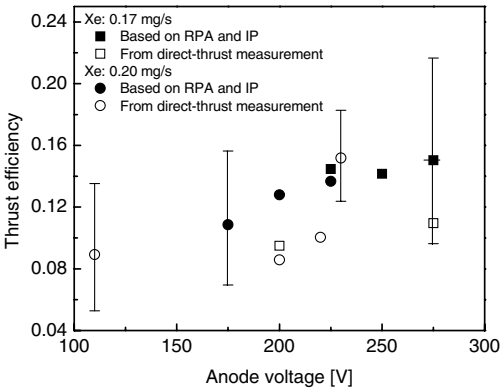

Fig. 15 Anode thrust efficiency as a function of the discharge voltage.

The variation in anode specific impulse with discharge voltage is shown in Fig. 16. The specific impulse is found to be in the range of 300–850 s for the test conditions, which can be compared with the 1500 s of the SPT-100 in nominal operating conditions [18]. This relatively low specific impulse is attributed to the relatively low ion energy (due to the 60 eV deficit) and large beam divergence in comparison to typical higher power thrusters. For our thruster, operation at higher specific impulses and higher thrust efficiencies requires high discharge voltages. However, thermal drifts and excessive heat transfer to the inner pole piece precluded operation at lower mass flow rates and higher discharge voltages, at this time. Future research will focus primarily on redesigning the discharge for improved thermal management of the inner pole piece and a reconfiguration of the magnetic circuit for optimization of the magnetic field.

IV. Summary

The operation and performance of a 4-mm-diam micro-Hall thruster was characterized, using measurements of ion current and ion energy in the plume, and thrust measurements (direct and indirect). The thruster was operated in the 10–40 W power range. The thrust was found to be in the range of 0.6–1.6 mN. Anode thrust efficiency is estimated to be 10–15% with an anode specific impulse in the range of 300–850 s.

In spite of the successful operation of this thruster, improvements are needed to increase performance. For long discharge operation (more than half an hour), thermal stress becomes a concern, which will necessitate an improved thermal design for heat removal from the magnetic structure. The alumina insulator ring could be replaced with a material with lower secondary electron emission (e.g., boron nitride) for increased discharge efficiency. The magnetic field shape and location relative to the channel could be optimized to reduce plume divergence and also increase efficiency. Finally, in our study, we have set aside the issue of the cathode/neutralizer, which is also difficult to scale down in size and power. Nevertheless, the results presented in this paper are encouraging, and it appears reasonable to foresee the design and operation of complete, 10 W class Hall thruster systems in the near future.

Acknowledgments

This research was supported in part by the National Science Foundation/Department of Energy Basic Plasma Initiative, and by the U.S. Air Force Office of Scientific Research. The authors would like to thank M. Bachand, C. Thomas, and E. Sommier for their technical assistance and helpful discussions. Partial support for Tsuyohito Ito was provided by the Japan Society for the Promotion of Science Postdoctoral Fellowships for Research Abroad program.

References

[1] Brown, C. O., and Pinsley, E. A., "Further Experimental Investigations of a Cesium Hall-Current Accelerator," *AIAA Journal*, Vol. 3, No. 5,

1965, pp. 853–859.
[2] Janes, G. S., and Lowder, R. S., "Anomalous Electron Diffusion and Ion Acceleration in a Low-Density Plasma," *Physics of Fluids*, Vol. 9, No. 6, 1966, pp. 1115–1123.
[3] Zhurin, D. P., Kaufman, H. R., and Robinson, R. S., "Physics of Closed Drift Thrusters," *Plasma Sources, Science and Technology*, Vol. 8, No. 1, 1999, pp. R1–R20.
[4] Meezan, N. B., Hargus, W. A., Jr., and Cappelli, M. A., "Anomalous Electron Mobility in a Coaxial Hall Discharge Plasma," *Physical Review E (Statistical Physics, Plasmas, Fluids, and Related Interdisciplinary Topics)*, Vol. 63, No. 2, 2001, pp. 026410.
[5] Fife, J. M., "Hybrid-PIC Modeling and Electrostatic Probe Survey of Hall Thruster," Ph.D. Thesis, Massachusetts Inst. of Technology, Cambridge, MA, 1998.
[6] Micci, M. M., and Ketsdever, A. D. (ed.), "*Micropropulsion for Small Spacecraft*," AIAA Progress in Astronautics and Aeronautics, Vol. 187, AIAA, Reston, VA, 2000.
[7] Guerrini, G., Vesselovzorov, A. N., Bacal, M., and Pokrovsky, I. B., "Investigation of a Small, Closed Electron Drift, Stationary Plasma Thruster," *Review of Scientific Instruments*, Vol. 67, No. 3, 1996, p. 990.
[8] Khayms, V., and Martinez-Sanchez, M., "Design of a Miniaturized Hall Thruster for Microsatellites," *32nd Joint Propulsion Conference*, AIAA Paper 96-3291, 1996.
[9] Khayms, V., "Advanced Propulsion for Microsatellites," Ph.D. Thesis, Massachusetts Inst. of Technology, Cambridge, MA, 2000.
[10] Schmidt, D. P., Meezan, N. B., Hargus, W. A., Jr., and Cappelli, M. A., "A Low-Power, Linear-Geometry Hall Plasma Source with an Open Electron-Drift," *Plasma Sources, Science and Technology*, Vol. 9, No. 1, 2000, pp. 68–76.
[11] Smirnov, A., Raitses, Y., and Fisch, N. J., "Enhanced Ionization in the Cylindrical Hall Thruster," *Journal of Applied Physics*, Vol. 94, No. 2, 2003, pp. 852–857.
[12] Smirnov, A., Raitses, Y., and Fisch, N. J., "Plasma Measurements in a 100 W Cylindrical Hall Thruster," *Journal of Applied Physics*, Vol. 95, No. 5, 2004, pp. 2283–2292.
[13] Smirnov, A., Raitses, Y., and Fisch, N. J., "Electron Cross-Field Transport in a Low Power Cylindrical Hall Thruster," *Physics of Plasmas*, Vol. 11, No. 11, 2004, pp. 4922–4933.
[14] Ito, T., and Cappelli, M. A., "A Low-Power Magnetized Microdischarge Ion Source," *Applied Physics Letters*, Vol. 89, 2006, p. 061501.
[15] Meeker, D. C., Finite Element Method Magnetics, Ver. 3.4.1, http://femm.foster-miller.net (retrieved 24 July 2007).
[16] Ito, T., Gascon, N., Crawford, W. S., and Cappelli, M. A., "Ultra-Low Power Stationary Plasma Thruster," International Electric Propulsion Conference Paper 2005-198, 2005.
[17] Gascon, N., Corey, R. L., Cappelli, M. A., and Hargus, W. A., Jr, "Hall Thruster with an External Acceleration Zone," International Electric Propulsion Conference Paper 2005-196, 2005.
[18] Gascon, N., Dudeck, M., and Barral, S., "Wall Material Effects In Stationary Plasma Thrusters 1: Parametric Studies of an SPT-100,", *Physics of Plasmas*, Vol. 10, No. 10, 2003, p. 4123.
[19] Barral, S., Makowski, K., Peradzynski, Z., Gascon, N., and Dudeck, M., "Wall Material Effects in Stationary Plasma Thrusters 2: Near-Wall and In-Wall Conductivity," *Physics of Plasmas*, Vol. 10, No. 10, 2003, p. 4137.
[20] Morozov, A. I., Esipchuk, Y. V., Kapulkin, A. M., Nevrovskii, V. A., and Smirnov, V. A., "Effect of Magnetic Filed on a Closed-Electron-Drift Accelerator," *Soviet Physics Technical Physics*, Vol. 17, No. 3, 1972, p. 482.
[21] Boeuf, J.-P., and Garrigues, L., "Low Frequency Oscillations in a Stationary Plasma Thruster," *Journal of Applied Physics*, Vol. 84, No. 7, 1998, p. 3541.
[22] Absalamov, S. K., Andreev, V. B., Colbert, T., Day, M., Egorov, V. V., Gnizdor, R. U., Kaufman, H., Kim, V., Koriakin, A. I., and Kozubskii, K. N., "Measurement of Plasma Parameters in the Stationary Plasma Thruster (SPT-100) Plume and Its Effect on Spacecraft Components," *28th AIAA/SAE/ASME/ASEE Joint Propulsion Conference*, AIAA Paper 92-3156, 1992.
[23] Hobbs, G. D., and Wesson, J. A., "Heat Flow Through a Langmuir Sheath in the Presence of Electron Emission," *Plasma Physics*, Vol. 9, No. 1, 1967, p. 85.
[24] Schwager, L. A., "Effects of Secondary and Thermionic Electron Emission on the Collector and Source Sheaths of a Finite Ion Temperature Plasma Using Kinetic Theory and Numerical Simulation," *Physics of Fluids B*, Vol. 5, No. 2, 1993, p. 631.
[25] Staack, D., Raitses, Y., and Fisch, N. J., "Temperature Gradient in Hall Thrusters," *Applied Physics Letters*, Vol. 84, No. 16, 2004, pp. 3028–3030.
[26] Bareilles, J., Hagelaar, G. J. M., Garrigues, L., Boniface, C., Boeuf, J. P., and Gascon, N., "Critical Assessment of a Two-Dimensional Hybrid Hall Thruster Model: Comparisons with Experiments," *Physics of Plasmas*, Vol. 11, No. 6, 2004, p. 3035.
[27] Scharfe, M. K., Gascon, N., Cappelli, M. A., and Fernandez, E., "Comparison of Hybrid Hall Thruster Model to Experimental Measurements," *Physics of Plasmas*, Vol. 13, Aug. 2006, p. 083505.
[28] Hofer, R., Haas, J., and Gallimore, A., "Ion Voltage Diagnostics in the Far-Field Plume of a High-Specific Impulse Hall Thruster," *39th Joint Propulsion Conference*, AIAA Paper 2003-4556, 2003.
[29] Hofer, R. R., Jankovsky, R. S., and Gallimore, A. D., "High-Specific Impulse Hall Thrusters, Part 1: Influence of Current Density and Magnetic Field," *Journal of Propulsion and Power*, Vol. 22, No. 4, 2006, pp. 721–731.
[30] Hofer, R. R., and Gallimore, A. D., "High-Specific Impulse Hall Thrusters, Part 2: Efficiency Analysis," *Journal of Propulsion and Power*, Vol. 22, No. 4, 2006, 732–740.

A. Gallimore
Associate Editor